Enabling direct compression tablet formulation of celecoxib by simultaneously eliminating punch sticking, improving manufacturability, and enhancing dissolution through co-processing with a mesoporous carrier

Shubhajit Paul, Yiwang Guo, Chenguang Wang, Jiangnan Dun, Changquan Calvin Sun*

Pharmaceutical Materials Science and Engineering Laboratory, Department of Pharmaceutics, College of Pharmacy, University of Minnesota, 9-127B Weaver-Densford Hall, 308 Harvard Street S.E., Minneapolis, MN 55455

*Corresponding author

Changquan Calvin Sun, Ph.D.

9-127B Weaver-Densford Hall

308 Harvard Street S.E.

Minneapolis, MN 55455

Email: sunx0053@umn.edu

Tel: 612-624-3722

Fax: 612-626-2125

ABSTRACT

The development of a high quality tablet of Celecoxib (CEL) is challenged by poor dissolution, poor flowability, and high punch sticking propensity of CEL. In this work, we demonstrate a particle engineering approach, by loading a solution of CEL in an organic solvent into a mesoporous carrier to form a coprocessed composite, to enable the development of tablet formulations up to 40% (w/w) of CEL loading with excellent flowability and tabletability, negligible punch sticking propensity, and a 3-fold increase in *in vitro* dissolution compared to a standard formulation of crystalline CEL. CEL is amorphous in the drug-carrier composite and remained physically stable after 6 months under accelerated stability conditions when the CEL loading in the composite was ≤ 20% (w/w). However, crystallization of CEL to different extents from the composites was observed under the same stability condition when CEL loading was 30-50% (w/w). The success with CEL encourages broader exploration of this particle engineering approach in enabling direct compression tablet formulations for other challenging active pharmaceutical ingredients.

KEYWORDS: Punch sticking, powder flow, dissolution rate, mesoporous carrier, direct compression.

1. INTRODUCTION

The tablet is the most commonly used pharmaceutical dosage form to treat or alleviate a disease condition in humans, because of better stability, higher patient-compliance, and lower manufacturing cost compared to other dosage forms (Arshad et al., 2021). Among the different processes for tablet manufacturing, direct compression (DC) is preferred if possible as the process is devoid of solvent usage and the most economical since it involves fewer steps than other processes. In fact, direct compression is an important route to continuous manufacturing of tablets meeting established quality standards (Lee et al., 2015). A successful DC process requires adequate tabletability and flowability of the formulations to ensure adequate mechanical strength and content uniformity of the finished dosage forms (C. C. Sun, 2010). In addition, formulation components should not stick to punches during compression, in order to meet aesthetic standards of the tablet appearance by avoiding dull appearance or pitted surface (Chattoraj et al., 2018). During large scale commercial manufacturing, such sticking problems must be eliminated in order to avoid stoppage of compression operations needed for cleaning and polishing of punches.

Celecoxib (CEL) is a non-steroidal anti-inflammatory drug (NSAID) frequently used in the treatment of osteoarthritis and rheumatoid arthritis. Tablet product development of CEL is challenging due to its poor dissolution performance (a weak acid with pK_a =11.1 and intrinsic solubility of 3-7 μg/mL in water) (Paulson et al., 2001) These problems have been addressed using several solubilizing strategies, such as solid dispersion by spray drying (Fouad et al., 2011), self-emulsifying drug delivery (Song et al., 2013), inclusion complexation (Sinha et al., 2005), pharmaceutically acceptable solvates (Wang and Sun, 2021), spherical crystallization (Paradkar et al., 2002) and nanoparticulates (Liu et al., 2010). Despite these efforts, tablet products of CEL are still not yet available. A successful commercial CEL tablet product requires effective resolution to these critical issues on manufacturability and slow dissolution.

Mesoporous materials have recently gained attention as a class of drug delivery carriers due to their high specific surface areas, tunable pore size to accommodate diverse active pharmaceutical ingredients (APIs), and excellent thermal stability (Bharti et al., 2015; Florek et al., 2017; Slowing et al., 2008). Additionally, amorphous APIs with acceptable physical stability can be achieved by confining API in the small pores of mesoporous carriers (Baumgartner and Planinšek, 2021; Zolotov et al., 2021), which could enhance API dissolution. Mesoporous carriers with different physico-chemical properties can be used to achieve flexibility in API loading without significantly impacting manufacturability or content uniformity (Sun et al., 2018). Here, we attempted to develop a DC tablet product of CEL by overcoming key manufacturability issues identified above, while simultaneously improving dissolution through using a CEL-carrier composite. We hypothesize that loading CEL inside a porous carrier would significantly reduce the probability of punch sticking by minimizing direct contact between CEL and punch surface during compression.

2. MATERIALS AND METHODS

2.1. Materials

Celecoxib (CEL, Form III, d_{50} = 11.2 μm) (Aarti Labs Pvt. Ltd., Karnataka, India) was used as received. The same lot of CEL was also used in previous punch sticking studies (Paul et al., 2017d, 2017b, 2017c). Neusilin® (US2, Fuji Chemical Industries PVt. Ltd., Toyama, Japan) was employed as a mesoporous carrier. Microcrystalline cellulose (MCC; Avicel PH102, FMC Biopolymer, Philadelphia, PA) and lactose monohydrate (LM; Fastflo®, Foremost Farms, Clayton, WI) were used as tablet filler. Croscarmellose sodium (NaCMC; Ac-Di-Sol, /FMC Biopolymer, Philadelphia, PA) was used as a tablet disintegrant. Magnesium stearate (MgSt; HyQual™, Mallinckrodt, St Louis, MO) was used as a lubricant. Dimethyl

formamide (DMF; Sigma Aldrich, Saint Louis, MO) was used as a solvent to prepare CEL solutions for loading into the carrier.

2.2. Methods

2.2.1. Loading CEL in the carrier

A constant ratio of Neusilin to solution 2:1 (w:v) was used so that solution fills most pores in Neusilin. An appropriate amount of CEL was first dissolved in DMF (a class II solvent) to form a solution with a desired concentration, which was then added dropwise into Neusilin while being mixed with a spatula. The concentration of CEL in DMF was varied to obtain 10-30% loading of CEL in Neusilin after drying. The moist powder was dried under house vacuum at 50°C overnight to remove DMF. Higher loadings of 40% and 50% CEL were achieved by repeated loading. The entrapment of CEL in Neusilin was expected to be essentially 100% since all of the solution went inside the carrier particles and CEL remained inside during drying. This was confirmed by extracting CEL from the composite using both methanol and ethanol (data not shown). The amount of residual DMF was not quantified in this work since it unlikely affects the assessed powder properties relevant to tablet manufacturing. However, residual solvents should be carefully monitored per the ICH guideline to make sure it does not exceed allowed safe levels in commercial tablets (ICH Guideline, 2021).

2.2.2. Powder blending, tableting, and sticking assessment

Five DC formulations prepared in this work comprised of two control formulations containing 20% as received crystalline CEL and three composite-based formulations (Table 1). CEL-Neusilin composites containing 10%, 30% and 50% CEL were used to prepare DC formulations containing 5%, 20% and 40% of overall CEL loading, respectively. These formulations contained 4% NaCMC as a disintegrant and 1% MgSt as a lubricant. All the

93 constituents were passed through a mesh #30 standard sieve before being blended in a mixer
94 (Turbula, Glen Mills Inc., Cliffton, NJ) for 3 min at 50 rpm. All blends were kept in ambient
95 temperature and 33% relative humidity (RH), over a saturated $MgCl_2$ solution (O'Brien, 1948),
96 for 2 days prior to compaction.

97 **Table 1.** Compositions of different DC formulations

Formulation	CEL (%)	CEL-Neusilin composite (%)	Neusilin (%)	MCC (%)	Lactose (%)	NaCMC (%)	MgSt (%)
Control 1	20	-	30	45	-	4	1
Control 2	20	-	-	45	30	4	1
Drug-carrier 5F	-	50 [a]	-	45	-	4	1
Drug-carrier 20F	-	66 [b]	-	29	-	4	1
Drug-carrier 40F	-	80 [c]	-	15	-	4	1

98 CEL loading in composite: *a* = 10%, *b* = 30%, and *c* = 50%.

99

100 Tablets were prepared by compressing a powder with a 9.5 mm flat-faced punches over
101 a pressure range of 25-300 MPa on a compaction simulator (Presster; Metropolitan Computing
102 Corp., NJ) at a tableting speed corresponding to 25 ms dwell time (corresponding to 49,300
103 tablets/h) by simulating Korsch XL100 press (10 stations).

104 Sticking assessment was conducted using an upper punch with a removable flat-faced
105 tip (round, 12.7 mm diameter) at a compaction pressure of 150 MPa to compress a total of 50
106 tablets for each formulation. The punch tip was removed and weighed after every 10 tablets to
107 determine the amount of mass adhered on to the punch face. After each removal, the punch tip
108 was weighed three times on a digital balance with precision of 0.01 mg and the average was
109 reported. The cumulative amount of mass adhered after 50 compactions was used to quantify
110 sticking propensity.

111 ***2.2.3. Powder flowability***

The flow properties of different formulations were accessed in triplicate using a ring shear cell tester under ambient condition (23°C and 20% - 25% RH). A preshear stress of 3 kPa was used with normal stress of 500, 1000, 1500, 2000 and 2500 Pa during shear testing to construct a yield locus. Unconfined yield strength (f_c) and major principal stress (σ_n) were obtained from each yield locus by drawing Mohr's circles. The flowability index, ff_c, was calculated using Eq. (1).

$$ff_c = \frac{\sigma_n}{f_c} \quad (1)$$

2.2.4. Powder true density determination

As water can be adsorbed by MCC, NaCMC and Neusilin, true density of each powder blend, ρ_t, was determined by nonlinear regression of tablet density (ρ) vs. P data according to Eq. 2 (Sun, 2004). This method was more suitable than helium pycnometry for determining true density of moisture-containing powders (Chang and Sun, 2017; C. (Calvin) Sun, 2005; Sun, 2008).

$$P = \frac{1}{C}\left[(1-\varepsilon_c) - \frac{\rho}{\rho_t} - \varepsilon_c \ln\left(\frac{1-\frac{\rho}{\rho_t}}{\varepsilon_c}\right)\right] \quad (2)$$

Accurate ρ_t is critical for calculating accurate ε using Eq. 3 for reliable analyses of powder compression performance (Paul et al., 2017a; C. C. Sun, 2005).

$$\varepsilon = 1 - \frac{\rho}{\rho_t} \quad (3)$$

2.2.5. Tablet diametrical breaking test

Tablets were broken on a texture analyzer (Texture Technologies Corp., Surrey, UK) at 0.01 mm/s. Using Eq. 4, tablet tensile strength (σ) was calculated from the breaking force (F), tablet diameter (D), and thickness (h) (Fell and Newton, 1970).

133 $$\sigma = \frac{2F}{\pi.D.h} \quad (4)$$

134 ***2.2.6. Compressibility analysis***

135 The tablet porosity (ε) - compaction pressure (P) data were analyzed by nonlinear
136 regression using Eq. 5 (Kuentz and Leuenberger, 1999).

137 $$P = \frac{1}{C}\left[\varepsilon - \varepsilon_c - \varepsilon_c \ln\left(\frac{\varepsilon}{\varepsilon_c}\right)\right] \quad (5)$$

138 A total of 12-15 tablets were compressed over 20-300 MPa for each formulation. Two
139 parameters, $1/C$ and ε_c, related to plasticity of the material and the critical porosity were
140 obtained from curve fitting (Paul and Sun, 2017; Sun, 2017).

141 ***2.2.7. Compactibility analysis***

142 Compactibility profile (σ vs. ε) of each formulation was analyzed by non-linear
143 regression of data using Eq. 6 (Ryshkewitch, 1953).

144 $$\sigma = \sigma_0 e^{-b.\varepsilon} \quad (6)$$

145 Where σ_0 is the maximum tensile strength of the tablet attained at zero porosity and b is an
146 empirical constant that quantifies sensitivity of σ to changes in ε. σ_0 can be used to quantify the
147 apparent bonding strength.

148 ***2.2.8. Expedited friability analysis***

149 A separate set of 12-15 tablets were compressed over 25-300 MPa pressure range and
150 subjected to impact and attrition in a friabilator (Pharma Alliance Group Inc., Model F2, Santa
151 Clarita, CA) for 4 min at 25 rpm. Each tablet was weighed before and after the test and the
152 percent weight loss for each tablet was determined and plotted against pressure to determine
153 the minimum pressure required for obtaining tablets with weight loss of less than 1.0%.

154 ***2.2.9. Solid State properties of the composites***

155 ***2.2.9.1. PXRD***

156 Samples of Neusilin loaded with different amounts of CEL were scanned over a 2θ
157 range of 5°–35° on a wide angle X-ray diffraction instrument (X'Pert Pro; PANalytical Inc.,
158 West Borough, MA) using Cu *K*α radiation (45 kV and 40 mA) at a step size of 0.0167° and a
159 dwell time of 1.15 s. The percent crystallinity of CEL in composites was determined by PXRD
160 from the calibration plot of total area of all peaks over the 2θ range of 5-35° as a function of
161 proportion of crystalline CEL (5-60%) in a physical mixture with Neusilin. All the
162 diffractograms were baseline corrected before peak area determination.

163 ***2.2.9.2. Thermal analyses***

164 Degradation temperature was determined using a thermogravimetry analyzer (Q50; TA
165 Instruments) by heating each sample at 10 °C/min to 350 °C. The maximum temperature in
166 subsequent DSC experiments was kept lower than the degradation temperature to avoid
167 contamination to the DSC cell of a differential scanning calorimeter (DSC; Q2000; TA
168 Instruments, New Castle, DE). Samples were heated to 180 °C at a heating rate of 10 °C/min
169 under 50 mL/min nitrogen gas purge. An empty aluminum pan was used as reference in all
170 cases.

171 ***2.2.9.3. Karl Fischer titration (KFT)***

172 KFT was performed using a Metrohm 831 KF coulometer, equipped with a Metrohm
173 703 Ti Stand mixer (Metrohm Inc., Riverview, FL, USA). Briefly, 50 mg of sample was
174 directly added to the thermostatic titration vessel containing reagent solution. The amount of
175 water in a sample is determined voltametrically by applying Faraday's law to calculate the
176 amount of water reacted with iodine, which is generated from an iodide containing reagent
177 under constant current. A start and stop drift of 10 µg/ min was used. Each sample was tested
178 in triplicate.

179 ***2.2.9.4. IR spectroscopy***

180 IR spectra of CEL, Neusilin, and 30% CEL loaded composite were recorded on a FTIR
181 spectrophotometer (Nicolet iS50; Thermo Scientific, Waltham, MA) with a built-in diamond
182 attenuated total reflection (ATR). Data was collected over the range of 400-4000 cm^{-1} at a
183 resolution of 4 cm^{-1} and 32 scans was processed to obtain an average spectrum using OMNIC
184 9.2 software.

185 ***2.2.9.5. Raman spectroscopy***

186 Raman spectra of CEL, Neusilin, and 30% CEL loaded composite were recorded on a
187 Raman microscope (Alpha300 R, WITec, Ulm, Germany). A point of interest in the powder
188 was focused with a 100x magnification lens and an average of two spectra was obtained using
189 a source laser (532 nm) at an integration time of either 1s (for CEL and carrier) or 10 s (for the
190 composite).

191 ***2.2.9.6. In vitro dissolution***

192 The *in vitro* dissolution of different formulations was evaluated using an artificial
193 stomach and duodenum (ASD) apparatus. It consists of two jacketed beakers with temperature
194 controlled at 37 °C by a water bath. This apparatus simulates stomach and duodenum fluid
195 transfer by regulating the flow using a programmatically controlled peristaltic pump
196 (Masterflex, L/S Easy-Load II, Cole-Parmer, Vernon Hills, IL).

197 To simulate human physiological conditions in the fast state, experiments were
198 conducted with 0.01 N HCl (pH = 2) for the stomach and 0.1 M sodium phosphate buffer (pH
199 = 6.8) for the duodenum. The initial volume of the stomach chamber was 250 mL, which was
200 decreased to 50 mL by first-order emptying with a half-life of 15 min. The duodenum volume
201 was maintained at 30 mL throughout the entire study, achieved by setting a vacuum line in the
202 duodenum chamber at a calibrated height. In addition, the chambers were infused with fresh

gastric or duodenal secretion liquid at 2 mL/min to mimic *in vivo* secretion processes. Drug concentration was monitored by a fiber optic UV/Vis probe. Mixing was achieved by an overhead paddle stirrer in the stomach chamber and a magnetic stirrer in the duodenum chamber. Calibration of all pumps and spectrometers were performed before each run. CEL release from the CEL-Neusilin 20F and Control 2 formulations were determined. Dissolution media were degassed to avoid generation of bubbles that might affect the real-time concentration detection with a UV dip probe.

2.2.9.7. Statistical analysis

The statistical mean difference between two set of data of interest was determined by student's t-test method at a statistical significance level of $p = 0.05$ using Origin Pro software (v17; Northampton, MA, USA).

3. RESULTS AND DISCUSSION

3.1. Baseline characterization of the carrier

Various mesoporous carriers from different manufacturers and different grades from the same manufacturer differ in solvent retention capacity (SRC) and compactibility. A greater SRC would allow a higher drug loading in the carrier while greater compactibility would favor the compression of tablets. We chose Neusilin US2, a magnesium aluminometasilicate, in this work because of its high SRC, neutral slurry pH (Sun et al., 2018), pharmaceutically acceptable safety profile for use in oral solid dosage form (Almotairy et al., 2023; Rowe et al., 2009), and excellent tabletability (Fig. 1a).

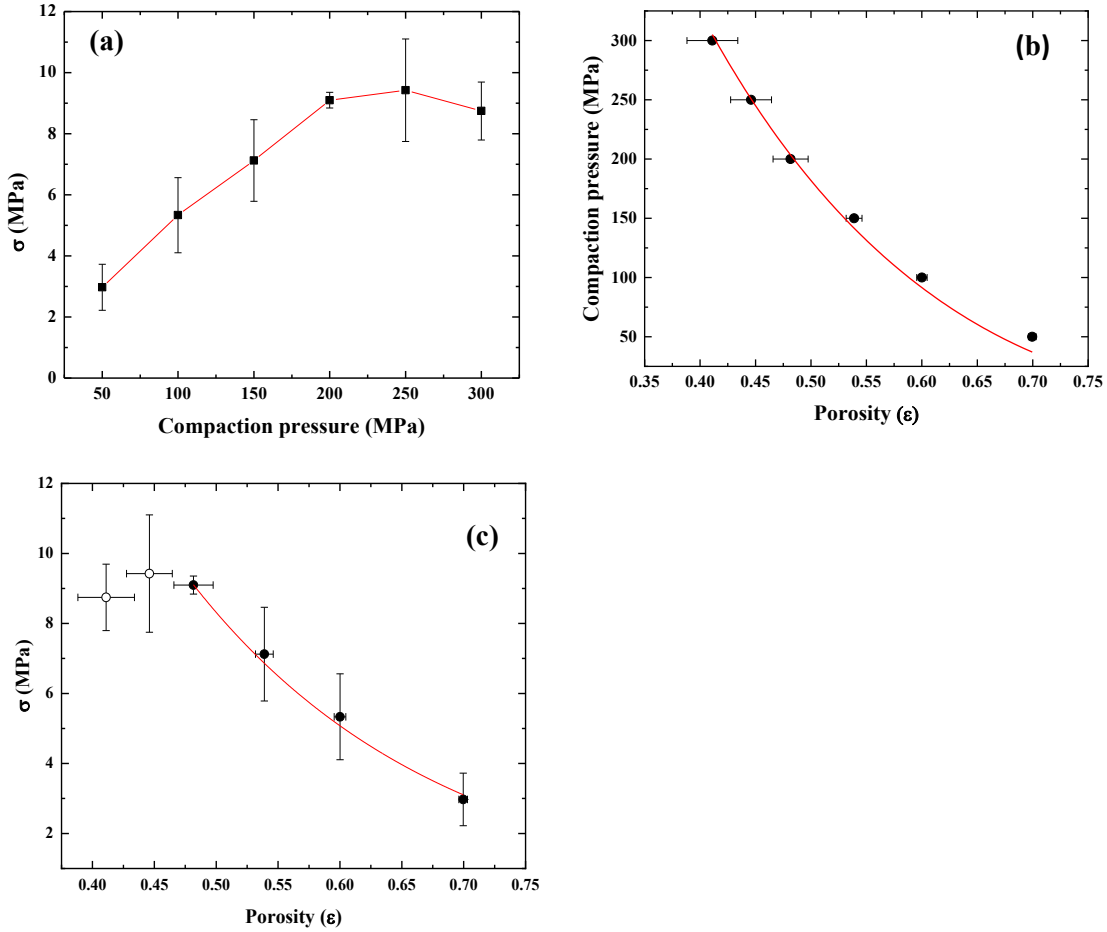

223

224 **Figure 1.** Compression properties of Neusilin US2 (n = 3), a) Tabletability, b) compressibility
225 and c) compactibility (two points at the lowest porosities were excluded from non-linear
226 regression because they are overcompressed).

227

228 Tablet porosity of Neusilin gradually decreases with increasing pressure, where a
229 porosity of 0.41 was attained at 300 MPa (Fig. 1b). The slow pore elimination of Neusilin
230 corresponds to a high $1/C$ value (1,409 ± 153 MPa). By this measure, Neusilin is significantly
231 harder than lactose ($1/C$ = 504 ± 19 MPa), significantly softer than anhydrous dicalcium
232 phosphate ($1/C$ = 4203 ± 77 MPa), but close to a 60% DCPA and 40% mixture with MCC ($1/C$
233 = 1117 ± 95 MPa) (Paul and Sun, 2017; Vreeman and Sun, 2021). To address the expected
234 high ejection force during manufacturing of tablets of hard materials (Sun, 2015), 1% MgSt
235 was incorporated in all formulations in this work. Neusilin also showed high apparent bonding
236 strength (σ_0) of ~90 MPa (Fig. 1c).

3.2. Impact of CEL loading on particle size and morphology

Neusilin particles are largely spherical, 50-100 μm in diameter, with many open pores visible under high magnification (Fig. 2a). Loading of CEL up to 30% (w/w) did not cause obvious change in the size and shape of Neusilin (Fig. 2), indicating CEL was loaded inside the pores of Neusilin, instead of coating Neusilin particles. However, slight size enlargement was observed for composites of 40% and 50% CEL loadings prepared by the process of repeated drug loading-drying cycles (Fig. 2). No difference in surface texture was observed in the composites up to 30% loading, with pores clearly visible without extraneous particles. However, some fiber-like CEL particles were observed at 40% and 50% loadings (Fig. 2b,c).

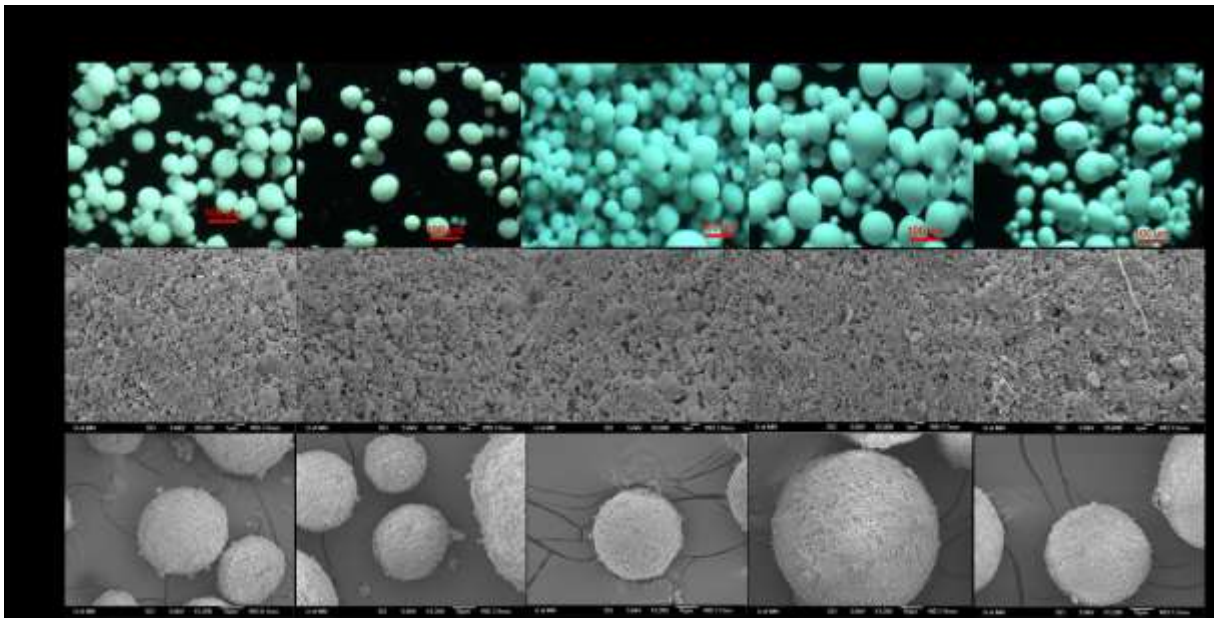

Figure 2. Morphology and surface textures of various CEL-Neusilin composites observed under (a) optical microscope (scale bar – 100 μm), and (b) SEM (scale bar = 1 μm), and (c) SEM (scale bar = 10 μm).

3.3. Solid-state properties of the composite

The absence of diffraction peaks in PXRD patterns suggests no crystalline CEL in composites, containing up to 50% CEL (Fig. 3a). The DSC thermogram showed no melting event for 30% CEL loaded composite. Melting of crystalline CEL (form III) at 160.8 °C was consistent as previously reported (Wang and Sun, 2019). The absence of X-ray diffraction peaks and melting events in the DSC thermograms of CEL-Neusilin composite also eliminate the possibility of a crystalline DMF solvate of CEL (Bond and Sun, 2020; Chawla et al., 2003).

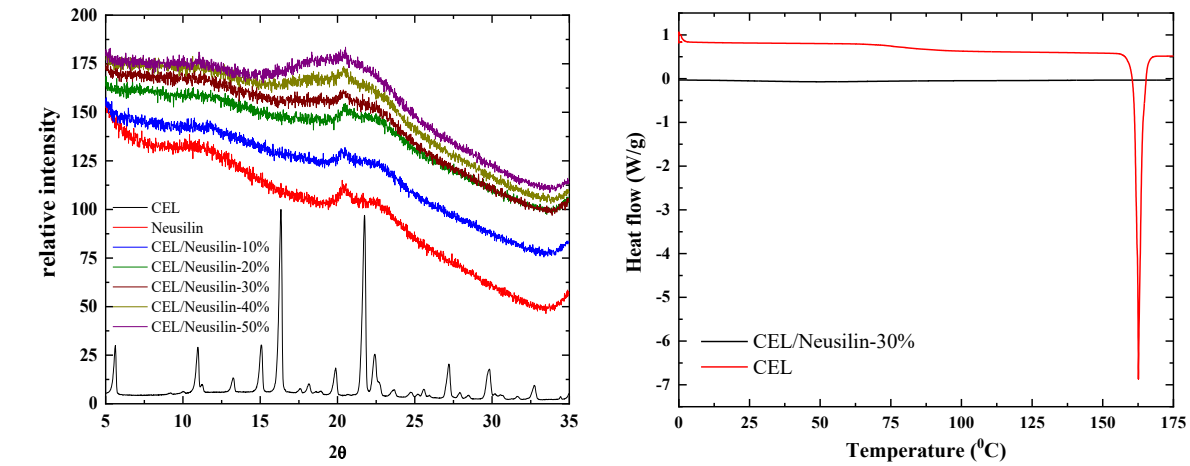

Figure 3. (a) X-ray diffractograms of CEL, Neusilin US2, and CEL-Neusilin composites (10-50% loading), (b) DSC thermograms of crystalline CEL and CEL-Neusilin composite at 30% loading.

The amount of DMF in the composite was probed by combining two methods, i.e. water content determination by KFT and weight loss by TGA. The as-received Neusilin had ~16% water content, which was slightly reduced to ~14% after vacuum drying (Fig. S2a). The CEL-Neusilin 30% composite had ~ 8% water content by KFT. The TGA data (Fig. S2b) indicates the corresponding weight loss of ~8% up to 220 °C, which is well above the boiling point of DMF (153 °C). These findings suggest that the amount of DMF solvent in the composite was negligible.

The IR spectra showed several signature peaks of the crystalline CEL and Neusilin (Fig. 4a). In CEL, the asymmetric and symmetric stretching frequencies of N-H were observed at 3332 and 3326 cm^{-1} and aromatic stretching of C-H at 3097 cm^{-1}. The S=O (1331 and 1062 cm^{-1}) and C-F stretching (1403 and 1374 cm^{-1}) and N-H bending (1596 and 1562 cm^{-1}) were also observed in the CEL fingerprint region. Neusilin exhibited broad O-H signature peak at 3415 cm^{-1}, corresponding to the presence of several silanol groups. In addition, a characteristic peak of Al-O-Si group was observed at 993 cm^{-1}. In contrast, the spectrum of CEL-Neusilin composite appears to be that of Neusilin overlaid with weak signals of CEL in the fingerprint region. This could be attributed to only 30% presence of CEL in the composite and limited penetration depth of the IR light rays into the composite particles, since CEL remains inside Neusilin particles.

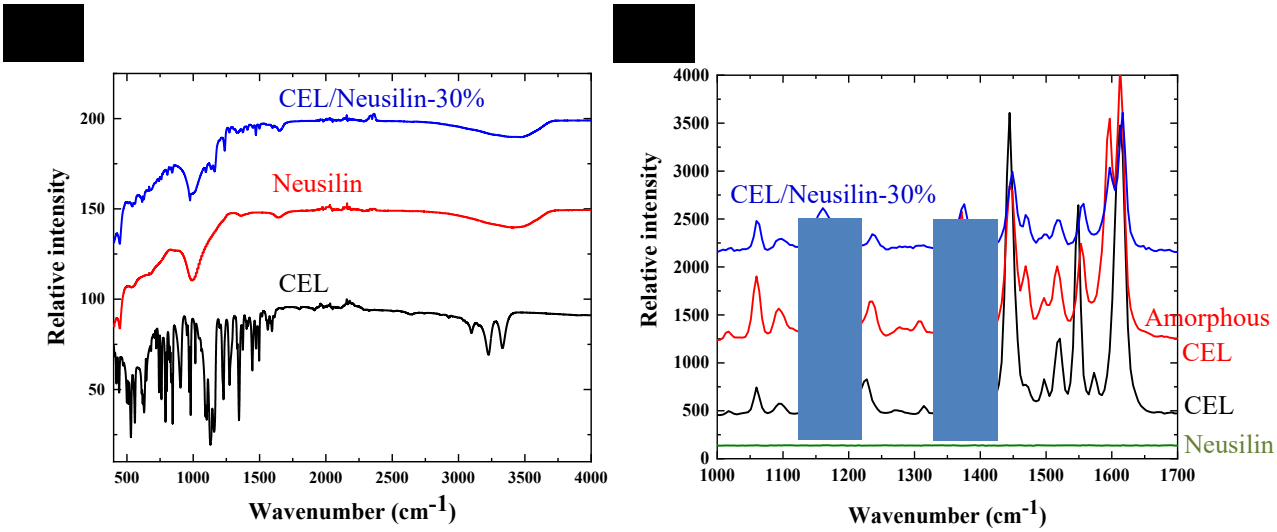

Figure 4. (a) IR and (b) Raman spectra for crystalline CEL, Neusilin, and CEL-Neusilin composite. Raman spectrum of amorphous CEL is shown for comparison, where regions of spectroscopic difference are shaded.

Raman spectra of various powders were also collected to further gain insights into the nature of CEL in the composites (Fig. 4b). Neusilin did not show any Raman signal. The

288 symmetric S=O stretching of crystalline CEL was observed at 1160-1200 cm^{-1} where
289 broadened peaks with low intensity were observed for CEL-Neusilin composite, matching with
290 that of amorphous CEL obtained by cryomilling. This is consistent with the amorphous nature
291 of CEL in the composite, suggested by PXRD and DSC. Similar observation was noted for C-
292 F stretching at 1230 cm^{-1} and N-H bending vibrations at 1560 cm^{-1} (Andrews et al., 2010). The
293 blue shift of N-H bending for both the composite and amorphous CEL to a higher frequency
294 suggests N-H groups are involved in stronger interactions than those in the crystalline CEL.
295 CEL in the composite and the amorphous form both exhibited a doublet around 1620 cm^{-1}
296 (Andrews et al., 2010), which could be ascribed to combined vibration of C-C with amino
297 stretching (Tammer, 2004). Overall, the spectroscopic data support that CEL inside Neusilin
298 particles is in amorphous state.

299 **3.4. Flowability of composite powders**

300 The flowability indices, ff_c, of all the composites were significantly higher than that of
301 Avicel PH102 (Fig. 5), implying excellent flowability (Sun CC, 2010). The ff_c values increased
302 with increasing CEL loading, which is in part due to increased particle density with increasing
303 CEL loading in Neusilin. This is confirmed by the increase in consolidated bulk density (CBD)
304 with increasing CEL loading (Fig. 5).

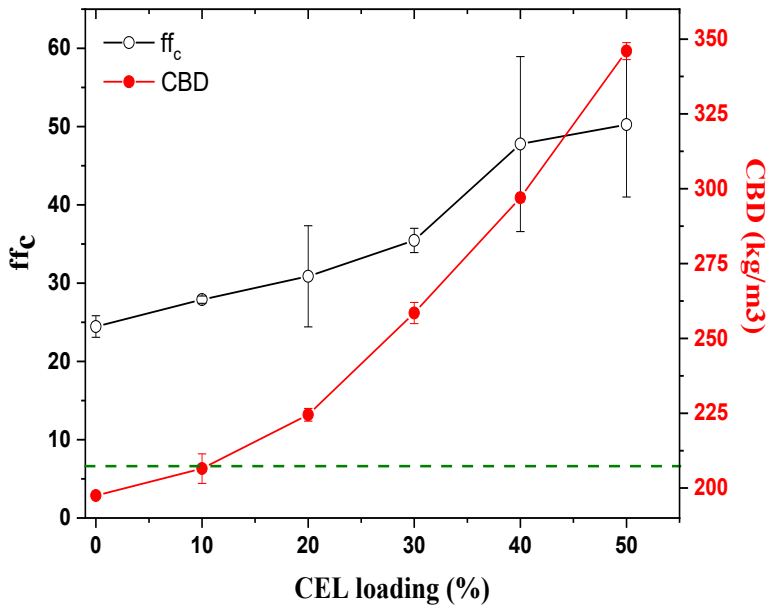

Figure 5. Flowability index and consolidated bulk density (CBD) of various Neusilin and CEL-Neusilin composites (n = 3). The horizontal dashed line indicates the *ff*c of Avicel PH102.

3.5. Physical stability of composites

The physical stability of composites with different CEL loadings was studied under accelerated stability conditions at 40 ºC/75% RH per the ICH guideline. Both open and closed vials were used to allow the separation of the influence of heat and moisture on physical stability of composites. After 3 months of exposure to the stressed stability conditions in both open and closed vials, 10% and 20% CEL loaded composites did not show any crystalline peaks in their X-ray diffractograms, indicating excellent physical stability (Fig. 6a,b). However, crystalline CEL peaks appeared for composites containing 30% or more CEL in both open and closed vials, where peak intensity increased with increasing CEL loading (Fig. 6a,b).

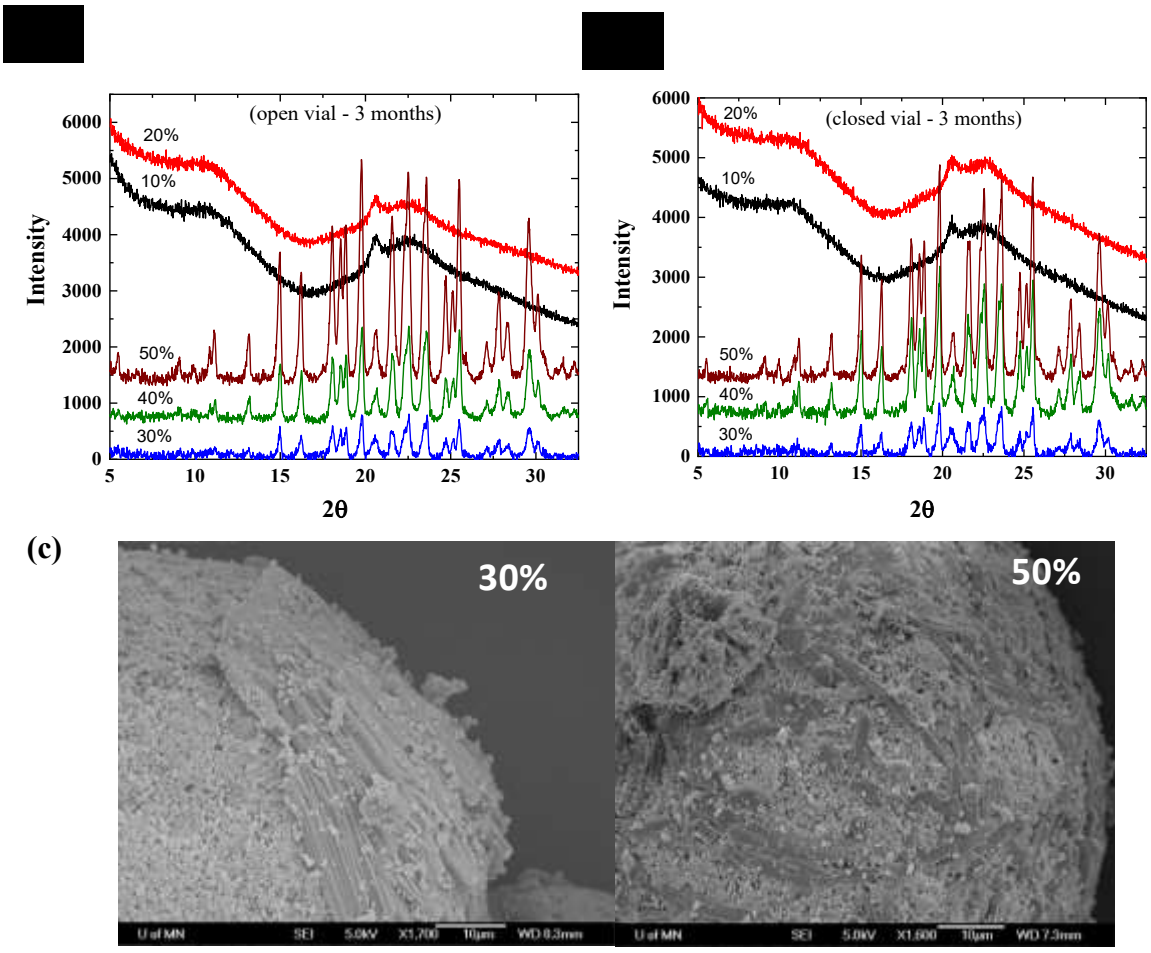

Figure 6. Different CEL-Neusilin after 3 months of exposure to stressed stability conditions (a) PXRD of samples under open conditions; (b) PXRD of samples under closed conditions and (c) SEM of samples under open conditions.

Using the calibration curve constructed with a set of physical mixtures of crystalline CEL and Neusilin in different proportions (Fig. S1a), the percent crystallinity of samples after storage under different stability conditions was estimated. Under open condition, the percent crystallized CEL at the end of a 3 months period, was essentially the same as that after 6 months (Table 2). Thus, crystallization of CEL had mostly completed after 3 months under this condition.

Table 2. Percent crystallinity of CEL-Neusilin composites under different stressed stability conditions.

CEL in composite (%)	% CEL crystallized			
	3 months		6 months	
	closed vial	open vial	closed vial	open vial
10	0	0	0	0
20	0	0	0	0
30	2.3 ± 0.02	2.6 ± 0.4	2.4 ± 0.01	2.6 ± 0.01
40	5.3 ± 0.8	7.9 ± 0.7	6.5 ± 0.3	7.6 ± 0.4
50	12.4 ± 1.8	14.8 ± 0.7	12.8 ± 1.3	13.5 ± 0.5

SEM revealed the appearance of elongated features on the surface of the carrier in the composites containing 30% and 50% CEL (Fig. 6c), which encompassed a greater area for 50% CEL composite. In combination with the X-ray data, these new features are attributed to crystalline CEL formed during stability storage. The crystallized CEL content increased with increasing CEL loading in the composites (Table 2). The extent of crystallization was only slightly lower in closed vials than that in open vials, implying that 75% RH only minimally impacted crystallization of amorphous CEL after a prolonged period. It is possible that crystallization at earlier time points could be faster under the open conditions. However, this requires a separate stability study to establish. It is useful to point out that the PXRD data suggested incomplete crystallization of amorphous CEL in 30%, 40%, and 50% CEL-loaded composites. For example, in 30% CEL-loaded composite after storage for 6 months, 2.4% (under closed conditions) and 2.6% (under open conditions) crystalline CEL was detected i.e. 27.6% and 27.4% of CEL remained amorphous. For the 40% CEL-loaded composite, 33.5% (closed vial) and 32.4% (open vial) CEL remained amorphous. Similarly, for the 50% CEL-loaded composite, 37.2% (closed vial) and 36.5% (open vial) CEL remained amorphous. These results are consistent with the observation that no crystalline CEL was detected in composites containing 10% and 20% CEL because they affirm that up to 27% amorphous CEL in composites remain physically stable even under stressed stability conditions.

3.6. Evaluation of the suitability of composites for DC formulations

Characterization results of the CEL-Neusilin composites suggest good physical stability and excellent powder properties, which make them suitable for developing a DC tablet formulation. To this end, the five DC formulations in Table 1 were prepared and systematically evaluated based on tablet manufacturability and key performance of tablets.

3.6.1. Flowability of formulations

For both control formulations, 20% CEL loading drastically reduces the flowability, despite only DC grade excipients with good flowability were used. The flowability of the control 1 formulation was comparable to that of Avicel PH102 (Fig. 7), indicating its marginal flowability for a high speed tableting process (Sun CC, 2010). When Neusilin was replaced by LM in the control 2 formulation, the flowability was significantly lower than that of Avicel PH102, indicating inadequate flowability to sustain a high speed tablet manufacturing process. In contrast, all three CEL-Neusilin composite based formulations had similar and excellent flow, as shown by very high ff_c values (Fig. 7). The flowability of these formulations are expected to be excellent for a high speed tablet manufacturing process. The insensitivity of flowability to CEL loading in composite is consistent with the fact that CEL remained in the pores of the carrier particles. Thus, its impact on the size and morphology of composite particles is small (Fig. 2).

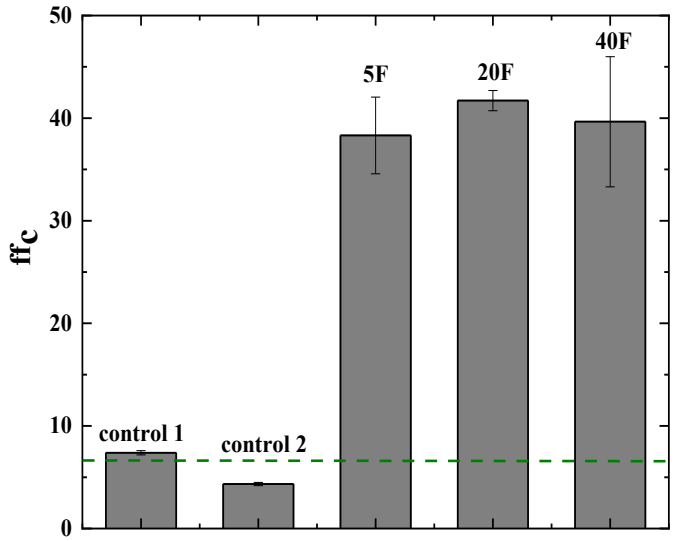

Figure 7. Flowability index of control and composite based CEL formulations (n = 3). The horizontal dashed line indicates the *ff*c of Avicel PH102.

3.6.2. Tableting performance of formulations

The tabletability of the five formulations followed the ascending order of control 2 < control 1 < CEL-Neusilin-40F < CEL-Neusilin -20F ≈ CEL-Neusilin-5F (Fig. 8a). The apparent bonding strength of the formulations, assessed by σ_0, also followed a similar order, control 2 < control 1 < CEL-Neusilin-40F < CEL-Neusilin-5F < CEL-Neusilin-20F (Fig. S3c and Table 3). The significantly better tabletability of control 1 formulation than control 2 formulation (Fig. 8a) is attributed to the excellent tabletability of Neusilin than lactose. Among the three composite based formulations, the tabletability of 5F and 20F formulation was similar in the entire pressure range (Fig. 8a). Tablet tensile strength of 40F formulation is similar to 5F and 20F formulations when compaction pressure is < 100 MPa, but significantly lower when pressure is > 150 MPa (Fig. 8a). It is useful to note that tablet porosity of the 40F formulation is always lower than that of 5F formulation, which means higher bonding area of the 40F formulation than the 5F formulation. Hence, the lower tabletability of the 40F formulation at

high pressures is attributed to its lower apparent bonding strength (Table 2), according to the bonding area-bonding strength interplay model (Osei-Yeboah et al., 2016; Paul et al., 2020).

Table 3. Compressibility and compactibility analysis of different formulations of CEL. Standard errors of fitting are shown in parentheses.

Formulations	KL fitting			Ryshkewitch fitting	
	1/C (MPa)	ε_c	R^2	σ_0 (MPa)	R^2
Control 1	292.0 (14.6)	0.82 (0.02)	0.997	11.7 (0.6)	0.97
Control 2	298.8 (16.2)	0.84 (0.02)	0.996	4.1 (0.06)	0.995
CEL-Neusilin-5F	199.9 (4.9)	0.88 (0.01)	0.999	38.5 (4.3)	0.968
CEL-Neusilin-20F	138.0 (13.9)	0.7 (0.04)	0.992	66.3 (10.7)	0.975
CEL-Neusilin-40F	379.4 (8.1)	0.89 (0.008)	0.999	20 (2.0)	0.961

As expected, friability is lower when tabletability is higher, owing to their stronger resistance to particle dislodging during impact (Fig. 8b). Only control 2 formulation showed more than 1.0% friability below 100 MPa pressure, while all other formulations could produce tablets that pass the USP friability criterion (< 1.0%) even when compressed at pressures as low as 25 MPa. The ability to make sufficiently strong tablets at relatively low pressures is beneficial for APIs that are sensitive to mechanical stress, such as solid form change (Fabbiani and Pulham, 2006) and loss of biological activities of therapeutic microbial or fragile proteins (Klukkert et al., 2015).

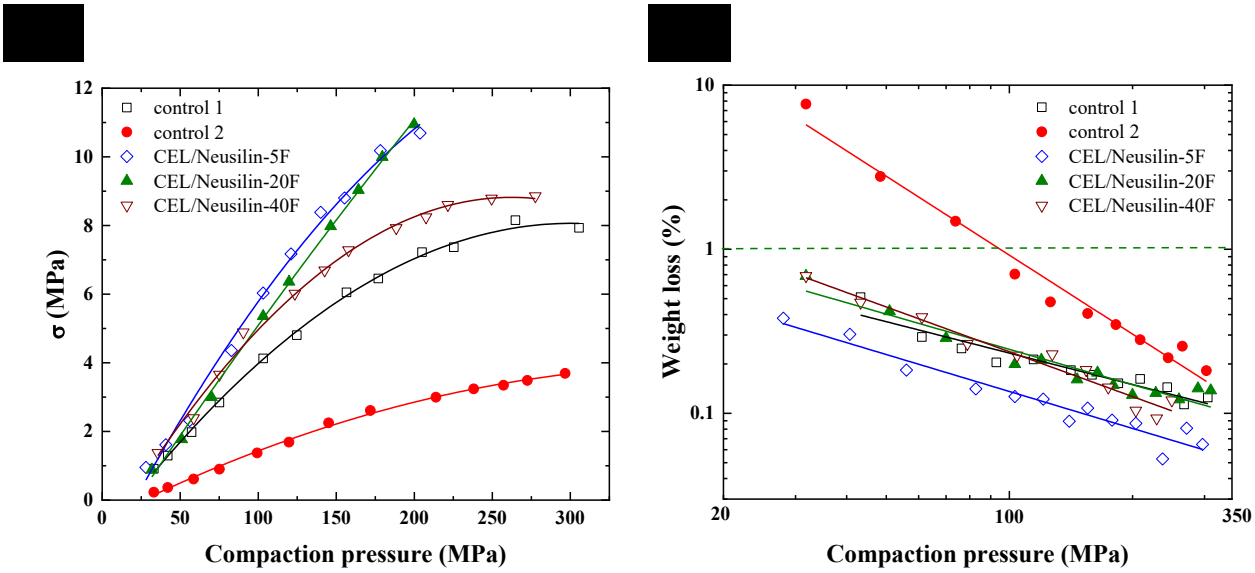

401

402 **Figure 8.** Tabletability (a) and friability (b) profiles of different formulations. Each point
403 represents result from a single tablet.

404

405 The consolidation behaviors of the five formulations differed as indicated by the
406 parameter 1/*C* (Table 3 and Fig. S3), which quantifies plasticity of a powder (Kuentz and
407 Leuenberger, 1999; Paul and Sun, 2017). By this measure, replacing LM with Neusilin did not
408 affect the deformability of Control 1 and 2 formulations because of their similar 1/*C* values
409 (Table 3). The plasticity of the three CEL-Neusilin composite based formulations follows the
410 order of 20F > 5F > 40F (Table 3). With a lower proportion of plastic MCC in the formulation,
411 the plasticity of CEL-Neusilin-20F formulation was surprisingly higher than 5F formulation.
412 A possible explanation is that a composite containing more CEL may be more plastic so that it
413 compensates the impact by the lower amount of MCC. However, the 1/*C* of CEL Neusilin-
414 40F (containing 80% of composite of 50% CEL loading) was higher than those of 5F and 20F
415 formulations. Thus, the overall plasticity of these formulations is a complex of interplay
416 between the impact of CEL loading on plasticity of the composite and weight fraction of the
417 composite in formulation. A dedicated study would be required to fully understand the
418 underlying mechanisms.

3.6.3. Punch sticking propensity of formulations

CEL exhibits a high punch sticking propensity, where severe punch sticking was observed in DC formulations at ≤ 20% CEL loading (Paul and Sun, 2018). Hence, punch sticking is a key manufacturing problem that must be addressed in order to develop a DC tablet formulation of CEL. The high sticking propensity of CEL was confirmed in this work using control formulations 1 and 2. The lower sticking propensity of control 1 is consistent with its higher tabletability (Fig. 8a). For the same API, a formulation having a stronger bonding among particles in tablet tends to exhibit lower punch sticking (Paul and Sun, 2018). However, punch sticking is still severe even for Control 1 formulation. In contrast, formulations of CEL-Neusilin composite exhibited no sticking to punch (clean punch tip after 50 tablets), even for the formulation containing 40% CEL (Fig. 9a). When all five formulations are considered, the severity of punch sticking followed a nonlinear negative dependence with σ_0 (Fig. 9b). Although the stronger bonding strength of the three composite based formulations does favor lower punch sticking propensity of CEL, a more important reason is the fact that CEL residing inside the pores of Neusilin does not come in contact with punch tip, unless extensive fracture of the composite particle occurred. Even in that case, the probability of CEL directly interacts with punch tip is still low. The assessment results clearly show that co-processing CEL with Neusilin is effective in mitigating, if not eliminating, punch sticking of CEL. The strategy should be universally applicable for reducing punch sticking problem of other APIs.

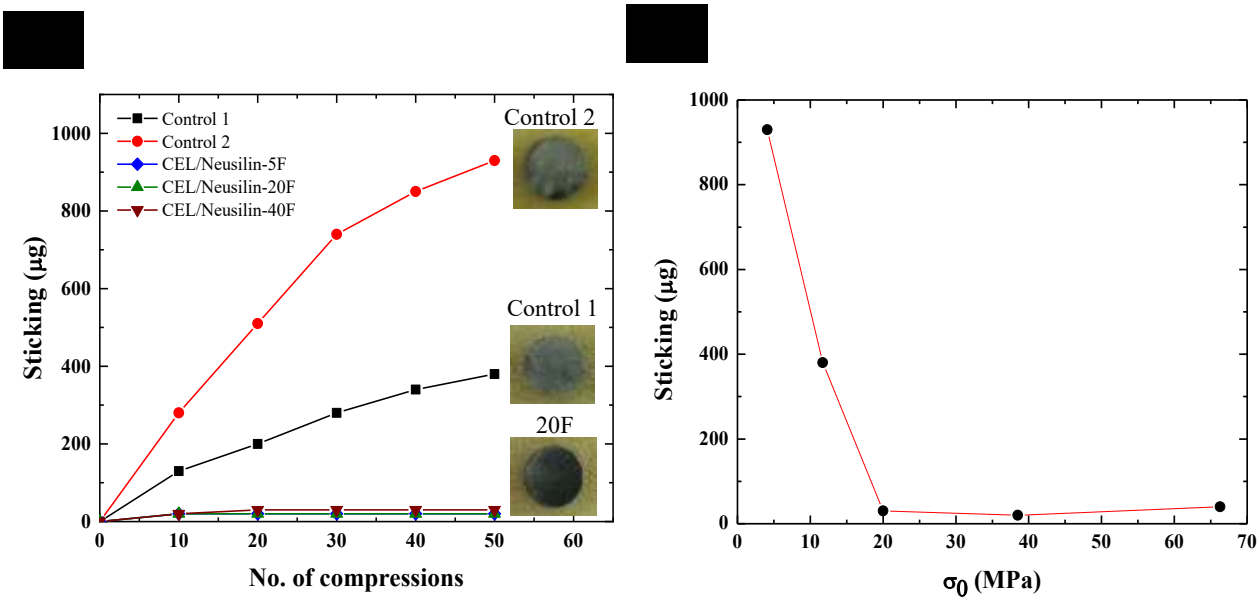

Figure 9. Dependence of sticking on (a) number of compressions (each point represents result from a single tablet.) and (b) bonding strength of five different DC formulations of CEL.

3.6.4. Dissolution performance of formulations

The dissolution performance of a representative composite based CEL tablet, CEL-Neusilin-20F, was evaluated using an artificial stomach and duodenum apparatus (ASD). The ASD more closely mimics the physiological conditions in human guts than the USP dissolution apparatus because it simulates the pH in stomach and duodenum and transfer both liquid and particles from stomach to duodenum. The drug concentration – time profile in the duodenum chamber was shown to be proportional to bioavailability of BCS class II APIs (Carino et al., 2010, 2006). Thus, it is a reliable *in vitro* dissolution method for rank ordering *in vivo* bioavailability of different formulations of the same BCS II API. At 20% loading, the dissolution profile of the CEL-Neusilin-20F composite formulation in the stomach chamber is higher than that of the control 2 formulation (Fig. 10a). The maximum CEL concentration at ~10 min is 4.3 µg/mL, which is 40% higher than the peak concentration at ~ 23 min for the control 2 formulation. The higher dissolution rate of the CEL-Neusilin formulation is attributed to the amorphous nature of CEL (Fig. 3). After 10 min, the CEL concentration

456 decreased quickly to become approximately the same as that from the control formulation at
457 30 min, indicating crystallization of CEL from the supersaturated solution.

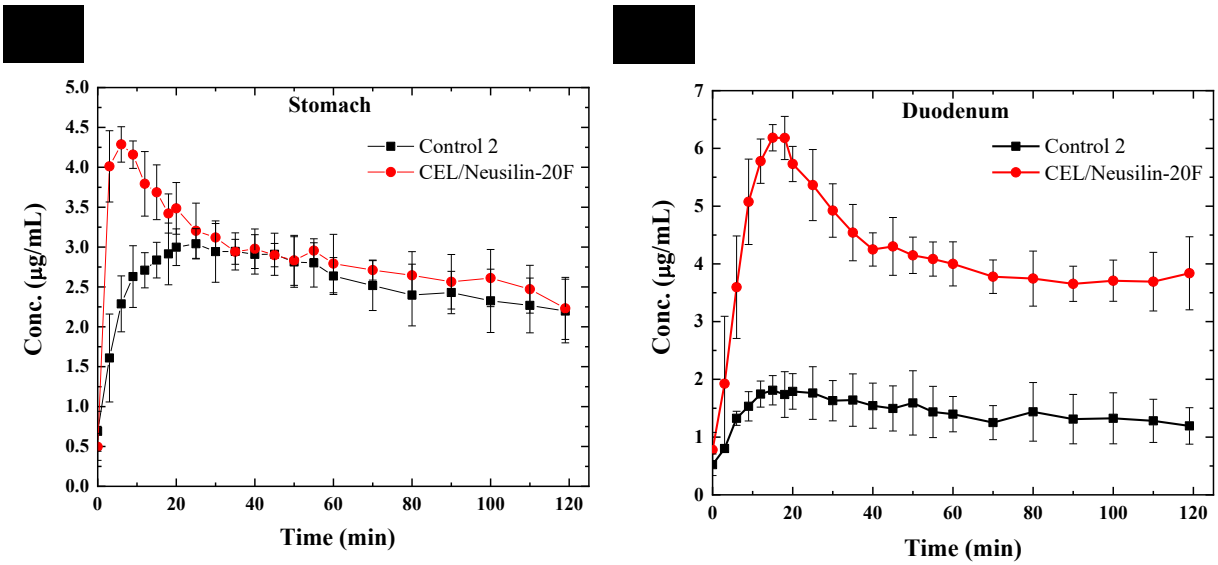

458

459 **Figure 10.** Dissolution profiles of tablets (n = 3) containing a total of 20% CEL (either CEL-
460 Neusilin or as-received) in (a) stomach chamber and (b) duodenum chamber.

461

462 The concentration-time profile of CEL in the duodenum chamber showed a marked
463 difference between the two formulations, where the composite based formulation showed
464 significantly higher concentration profile and the area under the time-concentration profiles
465 (AUC) (Fig. 10b). It reached a peak concentration of 6.5 μg/mL at ~20 min, which is more
466 than 3 times that of the control 2 formulation (2 μg/mL). The AUC of the CEL-Neusilin
467 composite based formulation (20F) is also approximately 3 times that of the control 2
468 formulation. Even without further formulation optimization, the composite based formulation
469 already exhibits much improved dissolution performance than the control formulation. If
470 desired, a higher CEL concentration of the composite based formulation could be achieved
471 through the general strategy of incorporating a sufficient amount of an effective precipitation

inhibitor in the formulation (Bi et al., 2011; Budiman et al., 2022; Guo and Sun, 2022; Ozaki et al., 2013; Yamashita and Sun, 2019).

4. Conclusion

This study shows the high potential of particle engineering to enable direct compression formulation of a challenging API, CEL, by forming composites with a mesoporous carrier. Up to 50% CEL could be loaded into Neusilin US2 by repeated loading, which remained amorphous after loading. Amorphous CEL undergoes partial crystallization under stressed conditions when the CEL loading was ≥30% (w/w), but remained physically stable at ≤ 20% CEL loading even under stressed stability conditions. When the composite was used in a formulation, flowability, tabletability, and punch sticking performance were all excellent, indicating a high possibility to developing a DC formulation amenable for high speed tablet manufacturing. By the measure of AUC in the duodenum, the bioavailability of the composite based tablet formulation (20% drug loading) is more than 3 times that of the formulation containing the same amount of crystalline CEL. Further property enhancement of the composite is possible, if needed. Thus, this approach may find broad applications in developing robust DC tablet formulations with excellent manufacturability and dissolution performance.

Acknowledgement

We thank Kunlin Wang for providing the Raman data of amorphous celecoxib.

REFERENCE

Almotairy, A., Almutairi, M., Althobaiti, A., Alyahya, M., Sarabu, S., Zhang, F., Bandari, S., Ashour, E., Repka, M.A., 2023. Investigation of hot melt extrusion process parameters on solubility and tabletability of atorvastatin calcium in presence of Neusilin® US2 79, 104075. https://doi.org/10.1016/j.jddst.2022.104075

Andrews, G.P., Abu-Diak, O., Kusmanto, F., Hornsby, P., Hui, Z., Jones, D.S., 2010. Physicochemical characterization and drug-release properties of celecoxib hot-melt extruded glass solutions. J Pharm Pharmacol 62, 1580–1590. https://doi.org/10.1111/j.2042-7158.2010.01177.x

Arshad, M.S., Zafar, S., Yousef, B., Alyassin, Y., Ali, R., AlAsiri, A., Chang, M.-W., Ahmad, Z., Elkordy, A.A., Faheem, A., Pitt, K., 2021. A review of emerging technologies enabling improved solid oral dosage form manufacturing and processing. Adv Drug Del Rev 178, 113840. https://doi.org/10.1016/j.addr.2021.113840

Baumgartner, A., Planinšek, O., 2021. Application of commercially available mesoporous silica for drug dissolution enhancement in oral drug delivery. Eur J Pharm Sci 167, 106015. https://doi.org/10.1016/j.ejps.2021.106015

Bharti, C., Nagaich, U., Pal, A.K., Gulati, N., 2015. Mesoporous silica nanoparticles in target drug delivery system: A review. Int J Pharm Investigation 5, 124–133. https://doi.org/10.4103/2230-973x.160844

Bi, M., Kyad, A., Kiang, Y.-H., Alvarez-Nunez, F., Alvarez, F., 2011. Enhancing and Sustaining AMG 009 Dissolution from a Matrix Tablet Via Microenvironmental pH Modulation and Supersaturation 12, 1157–1162. https://doi.org/10.1208/s12249-011-9679-x

Bond, A.D., Sun, C.C., 2020. Intermolecular interactions and disorder in six isostructural celecoxib solvates. Acta Crystallographica Section C 632–638. https://doi.org/https://scripts.iucr.org/cgi-bin/biblio_page?sk3751

Budiman, A., Citraloka, Z.G., Muchtaridi, M., Sriwidodo, S., Aulifa, D.L., Rusdin, A., 2022. Inhibition of Crystal Nucleation and Growth in Aqueous Drug Solutions: Impact of Different Polymers on the Supersaturation Profiles of Amorphous Drugs—The Case of Alpha-Mangostin. Pharmaceutics 14. https://doi.org/10.3390/pharmaceutics14112386

Carino, S.R., Sperry, D.C., Hawley, M., 2010. Relative bioavailability of three different solid forms of PNU-141659 as determined with the artificial stomach-duodenum model. J. Pharm. Sci. 99, 3923–3930. https://doi.org/10.1002/jps.22236

Carino, S.R., Sperry, D.C., Hawley, M., 2006. Relative bioavailability estimation of carbamazepine crystal forms using an artificial stomach-duodenum model. J. Pharm. Sci. 95, 116–125. https://doi.org/10.1002/jps.20495

Chang, S.-Y., Sun, C.C., 2017. Superior Plasticity and Tabletability of Theophylline Monohydrate. Mol Pharm, Mol Pharm 14, 2047–2055. https://doi.org/10.1021/acs.molpharmaceut.7b00124

Chattoraj, S., Daugherity, P., McDermott, T., Olsofsky, A., Roth, W.J., Tobyn, M., 2018. Sticking and Picking in Pharmaceutical Tablet Compression: An IQ Consortium Review. J. Pharm. Sci., Journal of Pharmaceutical Sciences 107, 2267–2282. https://doi.org/10.1016/j.xphs.2018.04.029

Chawla, G., Gupta, P., Thilagavathi, R., Chakraborti, A.K., Bansal, A.K., 2003. Characterization of solid-state forms of celecoxib. Eur J Pharm Sci 20, 305–317. https://doi.org/10.1016/s0928-0987(03)00201-x

Fabbiani, F.P.A., Pulham, C.R., 2006. High-pressure studies of pharmaceutical compounds and energetic materials. Chem Soc Rev 35, 932–942. https://doi.org/10.1039/b517780b

Fell, J.T., Newton, J.M., 1970. Determination of tablet strength by the diametral-compression test. J. Pharm. Sci. 59, 688–691. https://doi.org/10.1002/jps.2600590523

Florek, J., Caillard, R., Kleitz, F., 2017. Evaluation of mesoporous silica nanoparticles for oral drug delivery – current status and perspective of MSNs drug carriers. Nanoscale 9, 15252–15277. https://doi.org/10.1039/c7nr05762h

Fouad, E.A., EL-Badry, M., Mahrous, G.M., Alanazi, F.K., Neau, S.H., Alsarra, I.A., 2011. The use of spray-drying to enhance celecoxib solubility. Drug Dev Ind Pharm 37, 1463–1472. https://doi.org/10.3109/03639045.2011.587428

Guideline, ICH., 2021. IMPURITIES: GUIDELINE FOR RESIDUAL SOLVENTS Q3C(R8).

Guo, Y., Sun, C.C., 2022. Formulation strategies for mitigating dissolution reduction of p-aminobenzoic acid by sodium lauryl sulfate through diffusion layer modulation. Int J Pharm 611, 121310. https://doi.org/10.1016/j.ijpharm.2021.121310

Klukkert, M., Weert, M. van de, Fanø, M., Rades, T., Leopold, C.S., 2015. Influence of Tableting on the Conformation and Thermal Stability of Trypsin as a Model Protein 104, 4314–4321. https://doi.org/10.1002/jps.24672

Kuentz, M., Leuenberger, H., 1999. Pressure susceptibility of polymer tablets as a critical property: A modified heckel equation. J. Pharm. Sci. 88, 174–179. https://doi.org/10.1021/js980369a

Lee, S.L., O'Connor, T.F., Yang, X., Cruz, C.N., Chatterjee, S., Madurawe, R.D., Moore, C.M.V., Yu, L.X., Woodcock, J., 2015. Modernizing Pharmaceutical Manufacturing: from Batch to Continuous Production 10, 191–199. https://doi.org/10.1007/s12247-015-9215-8

Liu, Y., Sun, C., Hao, Y., Jiang, T., Zheng, L., Wang, S., 2010. Mechanism of dissolution enhancement and bioavailability of poorly water soluble celecoxib by preparing stable amorphous nanoparticles. J Pharm Pharm Sci 13, 589–606. https://doi.org/10.18433/j3530j

O'Brien, F E M, 1948. The Control of Humidity by Saturated Salt Solutions. Journal of Scientific Instruments 25, 73. https://doi.org/10.1088/0950-7671/25/3/305

Osei-Yeboah, F., Chang, S.Y., Sun, C.C., 2016. A critical examination of the phenomenon of bonding Area - bonding strength Interplay in powder tableting. Pharm. Res., Pharm Res 33, 1126–32. https://doi.org/10.1007/s11095-016-1858-8

Ozaki, S., Kushida, I., Yamashita, T., Hasebe, T., Shirai, O., Kano, K., 2013. Inhibition of crystal nucleation and growth by water-soluble polymers and its impact on the supersaturation profiles of amorphous drugs. Journal of Pharmaceutical Sciences 102, 2273–2281. https://doi.org/10.1002/jps.23588

Paradkar, A.R., Pawar, A.P., Chordiya, J.K., Patil, V.B., Ketkar, A.R., 2002. Spherical Crystallization of Celecoxib. Drug Dev Ind Pharm 28, 1213–1220. https://doi.org/10.1081/ddc-120015354

Paul, S., Chang, S.-Y., Sun, C.C., 2017a. The phenomenon of tablet flashing — Its impact on tableting data analysis and a method to eliminate it. Powder Technol, Powder Technology 305, 117–124. https://doi.org/10.1016/j.powtec.2016.09.054

Paul, S., Sun, C.C., 2018. Modulating Sticking Propensity of Pharmaceuticals Through Excipient Selection in a Direct Compression Tablet Formulation. Pharm Res, Pharm Res 35, 113. https://doi.org/10.1007/s11095-018-2396-3

Paul, S., Sun, C.C., 2017. The suitability of common compressibility equations for characterizing plasticity of diverse powders. Int J Pharm 532, 124–130. https://doi.org/10.1016/j.ijpharm.2017.08.096

Paul, S., Taylor, L.J., Murphy, B., Krzyzaniak, J., Dawson, N., Mullarney, M.P., Meenan, P., Sun, C.C., 2017b. Mechanism and Kinetics of Punch Sticking of Pharmaceuticals. J Pharm Sci, J Pharm Sci 106, 151–158. https://doi.org/10.1016/j.xphs.2016.07.015

Paul, S., Taylor, L.J., Murphy, B., Krzyzaniak, J.F., Dawson, N., Mullarney, M.P., Meenan, P., Sun, C.C., 2017c. Powder properties and compaction parameters that influence punch sticking propensity of pharmaceuticals. Int J Pharm, Int J Pharm 521, 374–383. https://doi.org/10.1016/j.ijpharm.2017.02.053

Paul, S., Wang, C., Sun, C.C., 2020. Tabletability Flip – Role of Bonding Area and Bonding Strength Interplay 109, 3569–3573. https://doi.org/10.1016/j.xphs.2020.09.005

Paul, S., Wang, K., Taylor, L.J., Murphy, B., Krzyzaniak, J., Dawson, N., Mullarney, M.P., Meenan, P., Sun, C.C., 2017d. Dependence of Punch Sticking on Compaction Pressure—Roles of Particle Deformability and Tablet Tensile Strength. J Pharm Sci, J Pharm Sci 106, 2060–2067. https://doi.org/10.1016/j.xphs.2017.04.059

Paulson, S.K., Vaughn, M.B., Jessen, S.M., Lawal, Y., Gresk, C.J., Yan, B., Maziasz, T.J., Cook, C.S., Karim, A., 2001. Pharmacokinetics of celecoxib after oral administration in dogs and humans: effect of food and site of absorption. J Pharmacol Exp Ther 297, 638–45.

RC, R., PJ, S., ME., Q., 2009. Handbook of Pharmaceutical Excipients.

Rowe, R.C., Sheskey, P.J., Quinn, M.E., 2009. Handbook of Pharmaceutical Excipients: 6th Edition.

Ryshkewitch, E., 1953. Compression Strength of Porous Sintered Alumina and Zirconia. J Am Ceram Soc 36, 65–68. https://doi.org/10.1111/j.1151-2916.1953.tb12837.x

Sinha, V.R., Anitha, R., Ghosh, S., Nanda, A., Kumria, R., 2005. Complexation of celecoxib with β-cyclodextrin: Characterization of the interaction in solution and in solid state. J. Pharm. Sci. 94, 676–687. https://doi.org/10.1002/jps.20287

Slowing, I.I., Vivero-Escoto, J.L., Wu, C.-W., Lin, V.S.-Y., 2008. Mesoporous silica nanoparticles as controlled release drug delivery and gene transfection carriers. Adv Drug Deliver Rev 60, 1278–1288. https://doi.org/10.1016/j.addr.2008.03.012

Song, W.H., Park, J.H., Yeom, D.W., Ahn, B.K., Lee, K.M., Lee, S.G., Woo, H.S., Choi, Y.W., 2013. Enhanced dissolution of celecoxib by supersaturating self-emulsifying drug delivery system (S-SEDDS) formulation. Arch Pharm Res 36, 69–78. https://doi.org/10.1007/s12272-013-0011-z

Sun, C. (Calvin), 2005. True Density of Microcrystalline Cellulose. J. Pharm. Sci., J Pharm Sci 94, 2132–2134. https://doi.org/10.1002/jps.20459

Sun, C. (Calvin), 2004. A Novel Method for Deriving True Density of Pharmaceutical Solids Including Hydrates and Water-Containing Powders. J. Pharm. Sci., J Pharm Sci 93, 646–653. https://doi.org/10.1002/jps.10595

Sun, C.C., 2017. Microstructure of Tablet—Pharmaceutical Significance, Assessment, and Engineering. Pharm Res, Pharmaceutical Research 34, 918–928. https://doi.org/10.1007/s11095-016-1989-y

Sun, C.C., 2015. Dependence of ejection force on tableting speed-A compaction simulation study. Powder Technol, Powder Technology 279, 123–126.

Sun, C. C., 2010. Setting the bar for powder flow properties in successful high speed tableting. Powder Technol, Powder Technology 201, 106–108. https://doi.org/10.1016/j.powtec.2010.03.011

Sun, Changquan Calvin, 2010. Setting the bar for powder flow properties in successful high speed tableting. Powder Technol, Powder Technology 201, 106–108. https://doi.org/https://doi.org/10.1016/j.powtec.2010.03.011

Sun, C.C., 2008. Mechanism of moisture induced variations in true density and compaction properties of microcrystalline cellulose. Int J Pharm, Int J Pharm 346, 93–101. https://doi.org/10.1016/j.ijpharm.2007.06.017

Sun, C.C., 2005. Quantifying Errors in Tableting Data Analysis Using the Ryshkewitch Equation Due to Inaccurate True Density. J Pharm Sci, J Pharm Sci 94, 2061–2068. https://doi.org/10.1002/jps.20421

Sun, W.-J., Aburub, A., Sun, C.C., 2018. A mesoporous silica based platform to enable tablet formulations of low dose drugs by direct compression. Int J Pharm 539, 184–189. https://doi.org/10.1016/j.ijpharm.2018.01.049

Tammer, M., 2004. G. Sokrates: Infrared and Raman characteristic group frequencies: tables and charts. Colloid Polymer Sci 283, 235–235. https://doi.org/10.1007/s00396-004-1164-6

Vreeman, G., Sun, C.C., 2021. Mean yield pressure from the in-die Heckel analysis is a reliable plasticity parameter. Int J Pharm 3, 100094.

Wang, K., Sun, C.C., 2019. Crystal Growth of Celecoxib from Amorphous State: Polymorphism, Growth Mechanism, and Kinetics. Crystal Growth & Design 19, 3592–3600. https://doi.org/10.1021/acs.cgd.9b00597

Wang, K., Sun, C.C., 2021. Direct compression tablet formulation of celecoxib enabled with a pharmaceutical solvate, Int J Pharm 596, 120239. https://doi.org/10.1016/j.ijpharm.2021.120239

Yamashita, H., Sun, C.C., 2019. Expedited Tablet Formulation Development of a Highly Soluble Carbamazepine Cocrystal Enabled by Precipitation Inhibition in Diffusion Layer. Pharm Res 36, 90. https://doi.org/10.1007/s11095-019-2622-7

Zolotov, S.A., Demina, N.B., Zolotova, A.S., Shevlyagina, N.V., Buzanov, G.A., Retivov, V.M., Kozhukhova, E.I., Zakhoda, O.Y., Dain, I.A., Filatov, A.R., Cheremisin, A.M., 2021. Development of novel darunavir amorphous solid dispersions with mesoporous carriers. Eur J Pharm Sci 159, 105700. https://doi.org/10.1016/j.ejps.2021.105700